Simulations of time-dependent fluorescence in nano-confined solvents

Ward H. Thompson
Department of Chemistry, University of Kansas, Lawrence, Kansas 66045

(Received 22 December 2003; accepted 9 February 2004)

The time-dependent fluorescence of a model diatomic molecule with a charge-transfer electronic transition in confined solvents has been simulated. The effect of confining the solvent is examined by comparing results for solutions contained within hydrophobic spherical cavities of varying size (radii of 10–20 Å). In previous work [J. Chem. Phys. **118**, 6618 (2002)] it was found that the solute position in the cavity critically affects the absorption and fluorescence spectra and their dependence on cavity size. Here we examine the effect of cavity size on the time-dependent fluorescence, a common experimental probe of solvent dynamics. The present results confirm a prediction that motion of the solute in the cavity after excitation can be important in the time-dependent fluorescence. The effects of solvent density are also considered. The results are discussed in the context of interpreting time-dependent fluorescence measurements of confined solvent systems.
 [DOI: 10.1063/1.1691391]

I. INTRODUCTION

There has recently been increasing interest in the chemical dynamics of confined solvents.[1–38] This derives from the ability of chemists to synthesize materials that are structured on the nanometer length scale[38–42] and the desire to use these materials to carry out useful chemistry or to understand the chemistry in similar systems found in nature. Despite the advances in synthetic techniques, our understanding of chemistry in solvents confined in nanometer-size cavities or pores is still relatively limited. Ultimately one would like to design nanostructured materials adapted for specific reactive or spectroscopic purposes, e.g., catalysis or sensing, by controlling the cavity/pore size, geometry, and surface chemistry. In order to develop guidelines for this design, we must first understand how the characteristics of a cavity affect the chemistry. These effects should be particularly pronounced when the chemical process of interest involves charge transfer and is therefore intimately coupled to the solvent dynamics.[43,44] Theoretical and simulation approaches can be useful in this context since the cavity properties (including size) can be straightforwardly controlled and varied, isolating their effects. This is the focus of this paper and a previous paper[45] (henceforth referred to as paper I).

One of the primary techniques for probing the change in solvent dynamics upon confinement is to measure the time-dependent fluorescence (TDF) of a dissolved chromophore.[46] Such measurements have been carried out by Levinger and co-workers in a wide variety of reverse micelles,[9–15] Bhattacharyya and co-workers in reverse micelles, vesicles, sol-gels, and zeolites,[4–8] Baumann *et al.* in sol-gels,[16,17] and a number of other groups.[18–25] In paper I we found that a chromophore with a charge transfer transition in a hydrophobic spherical nanometer-scale cavity displays different trends in the steady-state absorption and fluorescence spectra with cavity size. (The model solute, solvent, and nanocavity system are briefly described in Sec. II; additional details may be found in paper I.) Specifically, the fluorescence spectrum is redshifted as the cavity radius is increased while the absorption spectrum is essentially unchanged. This behavior can be understood based on the solute position: In the ground state the solute has a relatively small dipole moment and is most likely found near the cavity wall, excluded by the solvent. In the excited state, the solute dipole moment is large and the solute is most likely to be found fully solvated near the center of the cavity.[47] Thus, in paper I we predicted that the time-dependent fluorescence of such a chromophore in a spherical nanometer-scale cavity will exhibit characteristics due to the change in the chromophore position in the cavity after excitation. In this paper, we present nonequilibrium molecular dynamics simulations of the TDF spectra; the details of the calculations are given in Sec. III. In Sec. IV we present the results of the calculations that confirm this prediction, examine the relationship between the TDF spectra and cavity size, and compare with previous experimental and theoretical studies.

II. NANOCAVITY SYSTEM

In Sec. IV the results of simulations of a solute dissolved in a solvent confined inside a spherical nanocavity are presented. The solute is a model diatomic molecule (hereafter denoted as AB with Lennard-Jones and Coulombic interactions. The details of the model are given in paper I. Briefly, the A and B Lennard-Jones parameters are the same and are independent of electronic state. The two electronic states are related by a charge-transfer transition ($\mu_{gr}=1.44\,\mathrm{D}$, $\mu_{ex}=7.2\,\mathrm{D}$) with the excited state 2 eV higher in energy than the ground state. Though a two valence bond state model[48] is used the electronic coupling is sufficiently small (0.01 eV) that these simulations involve effectively fixed charges in the two electronic states. Simulations have been carried out with a CH_3I solvent using the rigid molecule model of Freitas *et al.*[49] for CH_3I ($\epsilon_{bulk}=7$). In this model the methyl group is treated as a ''unified atom.''

The model for cavity-molecule interactions is the same as in paper I.[32,33] The interactions of the solute and solvent molecules with the cavity walls involve only Lennard-Jones interactions.[32,33] The potential depends only on the radial distance of the Lennard-Jones site on the molecule from the center of the cavity. We consider two solvent densities, $\rho=1.4$ g/cm^3 and 2.0 g/cm^3 (the bulk density of CH_3I is 2.279 g/cm^3).[50] The density of the solution inside the cavity is taken to be approximately the same for a given solvent as the cavity size is varied. Note that the actual densities may be slightly less than these nominal densities since for a fixed cavity size it is not possible to attain an arbitrary density. The volume used in calculating this density is obtained by reducing the nominal cavity radius by $0.5\sigma_{\text{wall}}$ (σ_{wall} is the effective Lennard-Jones radius of the cavity wall) to approximately account for the excluded volume, a quantity that changes significantly with cavity size. The cavity radius, R_{cav}, is taken to be 10, 12, 15 Å for both densities and a 20 Å radius cavity is also considered for $\rho=1.4$ g/cm^3.

III. NONEQUILIBRIUM MOLECULAR DYNAMICS SIMULATIONS

A. Nanocavity simulations

Molecular dynamics (MD) simulations were carried out in the NVT ensemble. The time-dependent fluorescence simulations were initiated with a long equilibration run (1 ns) in the electronic ground state. The molecule was then promoted to the excited state and the fluorescence energy, $\Delta E_{\text{fl}}(t)=E_{\text{ex}}(t)-E_{\text{gr}}(t)$, was monitored as a function of time for 70 ps ($\rho=1.4$ g/cm^3) or 100 ps ($\rho=2.0$ g/cm^3). The system was then returned to its configuration just prior to excitation and propagated in the electronic ground state for 10 ps when the solute molecule was again excited and the TDF data collected. This process was repeated to obtain a total of 1200 nonequilibrium trajectories for each cavity and density. The TDF result can be plotted as the time-dependent Stokes shift, $\langle \Delta E_{\text{fl}}(t)-\Delta E_{\text{fl}}(0)\rangle$, or normalized in the usual way as

$$S(t)=\frac{\langle \Delta E_{\text{fl}}(t)-\Delta E_{\text{fl}}(\infty)\rangle}{\langle \Delta E_{\text{fl}}(0)-\Delta E_{\text{fl}}(\infty)\rangle}. \tag{3.1}$$

Here, $\Delta E_{\text{fl}}(\infty)$ is taken from an average of $\Delta E_{\text{fl}}(t)$ over the last 10 ps of the nonequilibrium dynamics. We have not accounted for any fluorescence lifetime.

In these systems there can be a significant difference between microcanonical (NVE) and canonical (NVT) results due to the small number of molecules (and perhaps the solvent-cavity interactions). Specifically, the absorption and fluorescence spectra and the TDF can all be different between the two ensembles. We have chosen to use an NVT ensemble in order to compare with our previous Monte Carlo simulations. However, the sensitivity of the results indicates that in some confined systems the particular ensemble appropriate to a specific experiment may not always be clear.

To sample a canonical ensemble we used a Nosé–Poincaré thermostat.[51] A Verlet leapfrog integrator was used with a time step of 1 fs. This approach has the advantage of providing a physical, evenly spaced time variable in the equations-of-motion. It is important to note that the NVT dynamics were used only for the equilibration stages with $T=298$ K. No thermostat was applied to the nonequilibrium dynamics during which the TDF signal was collected. The average temperature rose slightly during this period. Test calculations revealed only slight differences between this approach and an implementation of the thermostat for all dynamics.

B. Bulk simulations

We have also carried out nonequilibrium MD simulations in bulk CH_3I ($\rho=2.0$ g/cm^3) to provide a comparison with the nanocavity results. In these simulations 255 solvent molecules and one AB solute molecule were simulated with periodic boundary conditions. The box length was 31.12 Å and the interactions were smoothly truncated at a cutoff radius of 15.55 Å. (This treatment of the long-range interactions limits the usefulness of the bulk simulations to obtaining time scales for the time-dependent fluorescence; absolute fluorescence energies are not accurately reproduced.) A total of 160 nonequilibrium trajectories were propagated for 40 ps each using the same procedure described in Sec. III A.

IV. RESULTS

A. $\rho=1.4$ g/cm^3

We first consider the case of the solute dissolved in methyl iodide solvent at a relatively low density, 1.4 g/cm^3. (This was the density used to obtain most of the results in paper I.) The unnormalized and normalized time-dependent Stokes shift functions are shown for this system in Fig. 1. There are a couple of points to note regarding these results. First, $S(t)$ decays on multiple time scales. In fact, the decay is best fit by three exponentials,

$$S(t)=A_1e^{-t/\tau_1}+A_2e^{-t/\tau_2}+A_3e^{-t/\tau_3}, \tag{4.1}$$

with time scales of $\tau_1\sim 300$ fs, $\tau_2\sim 2.5$ ps, and $\tau_3\sim 15$ ps (see Table I). Second, there is no clear trend in $S(t)$ with cavity size, particularly for the radii larger than 10 Å. As is clear from the inset, this is true at both short and long times. From Table I it can be seen that the decay times, τ_i, in Eq. (4.1) are essentially independent of cavity size while the amplitudes, A_i, exhibit a weak, nonmonotonic dependence. There *is* a clear trend in the unnormalized TDF result since the Stokes shift increases with the cavity size.

Free energy surfaces shown in paper I indicate that after excitation the relaxation of the solvent polarization should be accompanied by solute motion (from near the cavity wall toward the interior). However, those Monte Carlo simulations could not address the time scale of the solute motion or how it affects $S(t)$. The solute position is obtained in the nonequilibrium MD simulations and the results are shown in Fig. 2, in which the average change in distance from the cavity wall, $\langle \Delta d(t)\rangle=\langle d(t)\rangle-\langle d(0)\rangle$, is plotted vs time for different cavity radii. In all cases the solute does, on average, move away from the cavity wall (toward the interior) with a time scale of ~15–25 ps (see Table II). This corresponds well to the longest time scale in the decay of the Stokes shift function in Fig. 1. It is important to note that the fluorescence

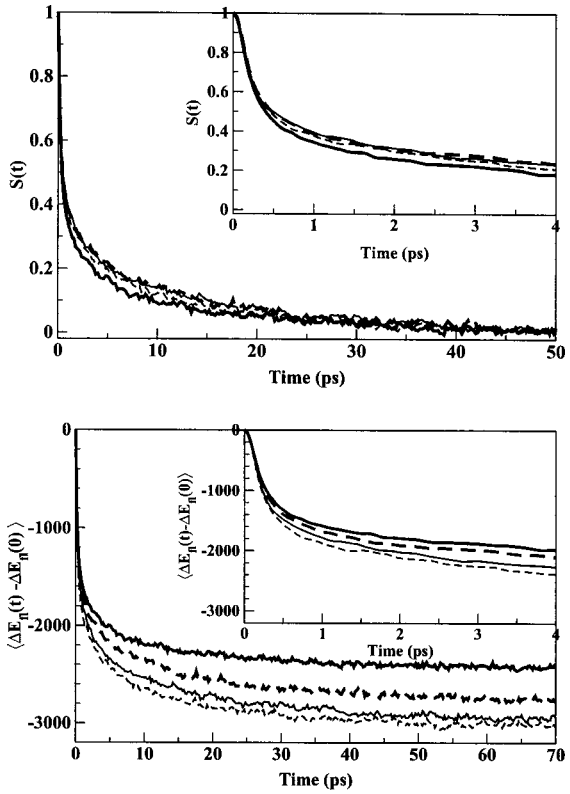

FIG. 1. The normalized (top) and unnormalized (bottom) time-dependent Stokes shift functions are plotted as a function of time for the solute in CH_3I with a density of 1.4 g/cm^3. Results are shown for cavities of radii 10 Å (thick solid line), 12 Å (thick dashed line), 15 Å (thin solid line), and 20 Å (thin dashed line). The short-time results are shown in the inset.

spectrum of the solute is strongly correlated with its position in the cavity. This is illustrated in Fig. 3, which shows the fluorescence spectra for solutes with fixed radial positions in a 15 Å radius cavity. (These spectra are obtained by Monte Carlo simulations in which the solute center-of-mass is fixed; details are given in Ref. 45.) The fluorescence spectrum shifts to longer wavelengths and broadens for solute positions further in the interior. It is also relevant that the shift begins to saturate as the radial distance is decreased, indicating the effect of solute motion on $S(t)$ is reduced for solutes in the cavity interior. Thus, the longest time scale for $S(t)$

TABLE I. The values obtained from fitting the time-dependent Stokes shift for ρ=1.4 g/cm^3 and 2.0 g/cm^3 by Eq. (4.1). (Error bars are based on estimated 95% confidence limits.)

R_{cav} (Å)	A_1	τ_1 (fs)	A_2	τ_2 (ps)	A_3	τ_3 (ps)
			ρ=1.4 g/cm^3			
10	0.60±0.02	293±30	0.23±0.03	2.8±0.5	0.17±0.04	16.2±3.0
12	0.56±0.02	301±30	0.19±0.03	2.7±0.6	0.25±0.04	16.5±2.5
15	0.52±0.02	271±40	0.23±0.03	2.2±0.5	0.25±0.04	16.2±2.5
20	0.57±0.02	286±40	0.21±0.03	3.0±0.7	0.22±0.04	14.7±2.5
			ρ=2.0 g/cm^3			
10	0.48±0.01	259±35	0.40±0.02	1.7±0.2	0.12±0.03	37.7±6
12	0.50±0.01	301±35	0.35±0.02	1.9±0.3	0.15±0.03	39.9±5
15	0.55±0.01	271±30	0.28±0.02	1.8±0.3	0.17±0.03	30.8±4
bulk	0.81±0.04	267±50	0.19±0.04	1.9±0.5	···	···

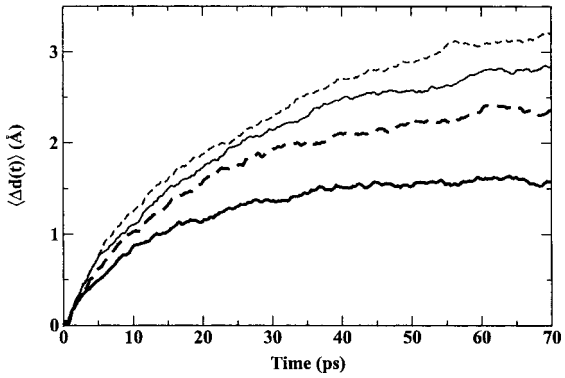

FIG. 2. The time-dependent solute position is shown as a function of time after excitation in CH_3I with a density of 1.4 g/cm^3. The position is plotted as the average change in the distance of the solute center-of-mass from the cavity wall and is shown for cavities with radii of 10 Å (thick solid line), 12 Å (thick dashed line), 15 Å (thin solid line), and 20 Å (thin dashed line).

decay should be somewhat shorter than that for the relaxation in the solute position and this is observed.

B. ρ=2.0 g/cm^3

We now consider results for a solute in a methyl iodide solvent nearer the bulk density. These simulations, which are more directly comparable to experimental measurements, address whether the qualitative behavior changes from the low density case and how the time scales for solvent relaxation and solute motion change with density. The unnormalized and normalized time-dependent Stokes shifts are shown in Fig. 4 for cavity radii of 10, 12, and 15 Å. As in the ρ=1.4 g/cm^3 case the time decay is multiexponential. Fits to $S(t)$ using Eq. (4.1) yield time constants of $\tau_1 \sim 300$ fs, $\tau_2 \sim 2$ ps, and $\tau_3 \sim 30-40$ ps (see Table I). As for the lower density, there is not a straightforward dependence of $S(t)$ on cavity size while the unnormalized Stokes shift again increases with cavity size. The fastest two decay times, τ_1 and τ_2, are independent of cavity size while τ_3 is smaller for the R_{cav}=15 Å cavity (see Table I). In contrast to the lower den-

TABLE II. Values obtained from fitting the average time-dependent solute position, $\langle \Delta d(t) \rangle$ after excitation for ρ=1.4 g/cm^3 and 2.0 g/cm^3. (Error bars are based on estimated 95% confidence limits.)

	$\langle \Delta d(t) \rangle = D(1-e^{-t/\tau_d})$	
R_{cav} (Å)	D	τ_d (ps)
10	1.60±0.03	14.2±1.0
12	2.40±0.04	18.7±1.0
15	2.90±0.05	21.3±1.0
20	3.32±0.05	23.7±1.1

	$\langle \Delta d(t) \rangle = D(1-B_1 e^{-t/\tau_{d1}} - B_2 e^{t/\tau_{d2}})$				
R_{cav} (Å)	D	B_1	τ_{d1} (ps)	B_2	τ_{d2} (ps)
10	3.44±0.06	0.046±0.003	1.4±0.4	0.954±0.003	342±9
12	2.39±0.03	0.065±0.005	1.4±0.5	0.935±0.005	119±2
15	2.60±0.03	0.066±0.006	1.5±0.6	0.934±0.006	72±2

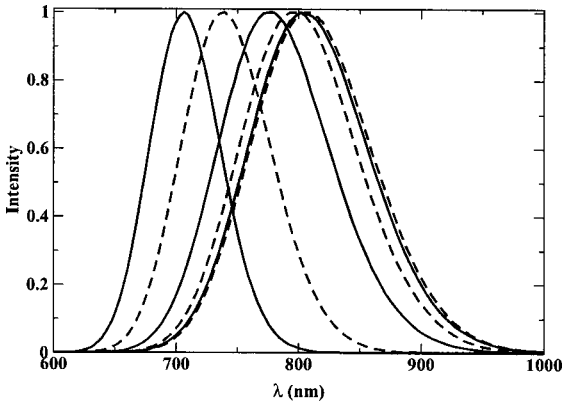

FIG. 3. Fluorescence spectra for solutes held at fixed distances from the cavity center for a 15 Å radius cavity, ρ=1.4 g/cm^3. The solid (dashed) lines represent distances from the cavity wall of 3, 7, and 11 Å (5, 9, 13 Å) from left to right.

sity case, the amplitudes, A_i, have a monotonic dependence on cavity size with A_1 and A_3 increasing with $R_{\rm cav}$ and A_2 decreasing.

The average change in solute position after excitation is shown in Fig. 5. Clearly the solute moves toward the center of the cavity on the time scale of the decay of $S(t)$. In comparison to the ρ=1.4 g/cm^3 results the solute motion is significantly slower (relaxation to the excited state equilibrium distribution is not completed in the 100 ps duration of the nonequilibrium trajectories) and it has a distinct biexponential time-dependence with a fast, but small, initial change in ~1.5 ps followed by much slower relaxation to the equilibrium solute position distribution for the excited state (see Table II). Since the nonequilibrium MD simulations do not extend to long enough times to recover the final, excited state solute distribution the fits in Table II, particularly D and τ_{d2}, should be considered only as rough guides. In contrast to the lower density case, the solute motion becomes faster as the cavity radius is increased.

V. DISCUSSION

The time-dependent Stokes shift results presented in Sec. IV display a number of interesting features including decay on multiple time scales, no clear trend with cavity size, and changes with solvent density. In this section we discuss these issues and compare the results to previous theoretical and experimental work.

We begin by a general discussion of the three time scales observed in the decay of $S(t)$. The fast time scale (~300 fs) in the time-dependent Stokes shift can be attributed to the inertial response of the solvent to the change in solute charge distribution.[46] At short times $S(t)$ is actually Gaussian (see the insets of Figs. 1 and 4) consistent with inertial dynamics; the exponential fit in Eq. (4.1) is used only to determine a rough time scale. The longest time scale of ~15–25 ps for ρ=1.4 g/cm^3 and ~30–40 ps for ρ=2.0 g/cm^3 is related to the solute motion after excitation. This is supported by the results for $\langle \Delta d(t) \rangle$ shown in Figs. 2 and 5. The intermediate time scale of ~1.5–3 ps is not as easily attributable though it likely involves primarily solvent reorientation since (1) a

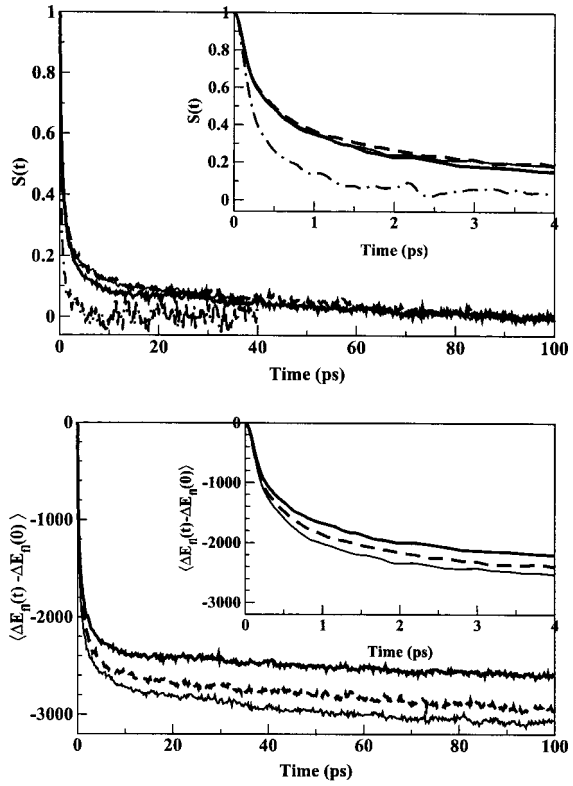

FIG. 4. Same as Fig. 1 but for CH_3I with a density of 2.0 g/cm^3. [No results are shown for the cavity radius of 20 Å and $S(t)$ results are shown by the dotted–dashed line for the bulk solvent case.]

similar time scale is observed as the long-time component in the bulk solvent $S(t)$ (see Fig. 4 and Table I), and (2) the solute position changes only slightly on this time scale. Naturally, the contributions of solute motion and solvent response to the time-dependent Stokes shift are convoluted, i.e., as the solute moves toward the cavity interior while the solvent molecules are continually reorienting in response. Thus, our discussion is subject to the caveat that it is not possible to unambiguously identify each time scale in the decay of $S(t)$ with that of the solute motion or solvent reorientation *alone*.

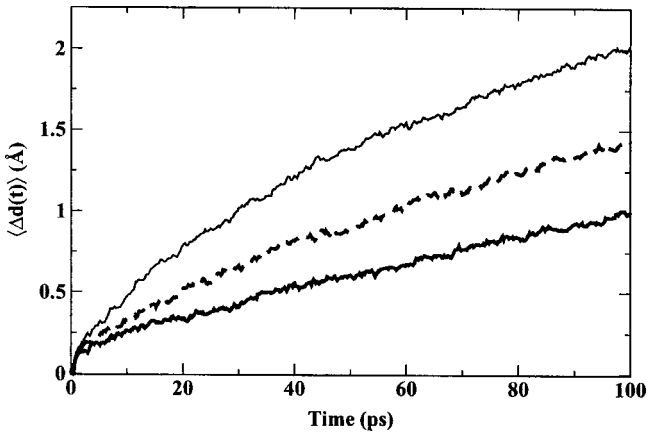

FIG. 5. Same as Fig. 2 but for CH_3I with a density of 2.0 g/cm^3. (No results are shown for cavity radius of 20 Å.)

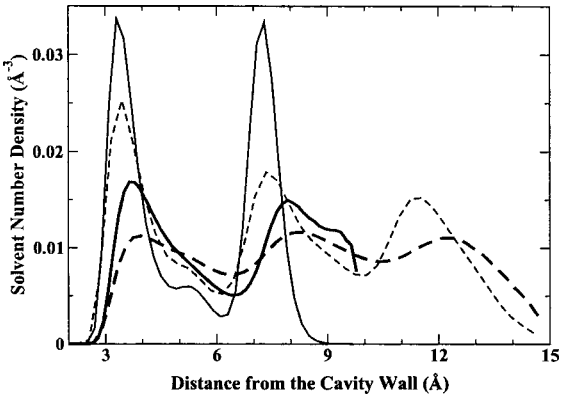

FIG. 6. The solvent radial density obtained from Monte Carlo simulations is shown as a function of position in the cavity for $\rho=1.4$ g/cm^3, $R_{cav}=10$ Å (thick solid line) and 15 Å (thick dashed line) and $\rho=2.0$ g/cm^3, $R_{cav}=10$ Å (thin solid line) and 15 Å (thin dashed line).

A. $\rho=1.4$ g/cm^3

Additional insight into the nonequilibrium dynamics for the low density case can be obtained by dividing up the contributions to $S(t)$ based on the solute position at the time of excitation. In particular, there is a natural dividing point presented by the solvent layering induced by the cavity wall. This well-known phenomenon also affects the solute position distribution (through the solute–solvent interactions) as was previously observed.[45] The solvent radial density is shown in Fig. 6 for different densities and cavity sizes. The solvent layering induced by the cavity wall is clearly observable and the density modulations decrease as the cavity size increases and as the total solution density decreases. Given this solvent density the nonequilibrium trajectories can be divided into those with solutes starting in the first solvent layer next to the wall, shown in the top panel of Fig. 7, and those beginning in the interior, shown in the bottom panel of Fig. 7. The dividing radius is taken to be 6.5 Å, based on the solvent density in Fig. 6 and Fig. 2 of paper I. (Note that a total of 1200 trajectories are divided in this way so that the number of trajectories differs between the panels of Fig. 7 and varies with cavity size.)

The time-dependent Stokes shift functions obtained by dividing the trajectories in this way *do* display a clear, though not dramatic, trend with cavity size. For trajectories starting near the cavity wall, $S(t)$ decays more slowly the larger the cavity size. The decay for these trajectories is also best fit by three exponentials, with time scales comparable to those obtained for the total $S(t)$. The primary differences between these results and the total $S(t)$, are in the amplitudes, A_i, in Eq. (4.1). In fact, the decay times, τ_i are quite similar for the different cavity sizes. The difference in amplitudes is related to the overlap of the ground and excited state solute position distributions in the cavity. This gives, in general, larger amplitudes for the "slow" component, A_3, the larger the cavity size. That is, if the ground and excited state distributions are identical, there will be no change in the average solute position and $A_3 \simeq 0$, whereas if the distributions are widely different A_3 will be large. As is evident from the Monte Carlo simulations presented in paper I, the overlap

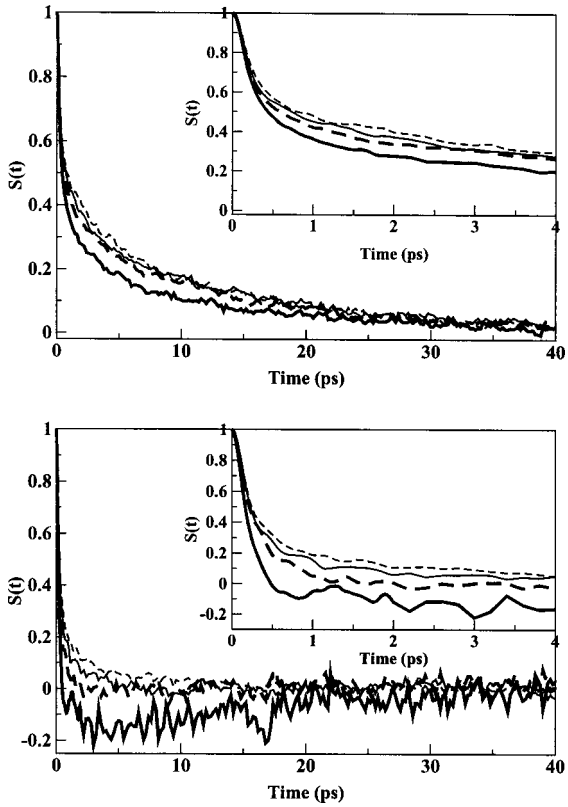

FIG. 7. The time-dependent Stokes shift is plotted for (top panel) solutes in the first solvent shell next to the cavity wall when excited, and (bottom panel) the remaining solutes that are in the cavity interior when excited. The results are for a solute in CH_3I ($\rho=1.4$ g/cm^3) and are shown for $R_{cav}=10$ Å (thick solid line), 12 Å (thick dashed line), 15 Å (thin solid line), and 20 Å (thin dashed line).

of these distributions is greater for smaller cavities and this is reflected in the increasing A_3 with increasing R_{cav}. The same argument applies for trajectories beginning near the wall with the modification that the overlap of the distributions in this first solvent layer is most relevant.

The $S(t)$ obtained from nonequilibrium trajectories starting in the cavity interior is more strongly dependent on cavity size. [Note that there is greater statistical error for these cases since $S(t)$ is constructed from only 58, 115, 243, and 439 trajectories for $R_{cav}=10$, 12, 15, and 20 Å, respectively. Thus, we focus on only the gross features.] One reason is that for $R_{cav}=10$, 12, and 15 Å the solute moves *toward* the cavity wall on average after excitation in these trajectories while for $R_{cav}=20$ Å the solute moves away from the cavity wall. This is shown in Fig. 8 which also clearly displays the significant dependence of solute motion on cavity size for trajectories starting in the interior. This solute motion leads to a significant negative lobe (that decays on an ~20 ps time scale) in $S(t)$ for $R_{cav}=10$ Å, a small negative lobe for 12 Å, and nearly double-exponential decay for 15 and 20 Å.

B. $\rho=2.0$ g/cm^3

In contrast to the $\rho=1.4$ g/cm^3 case, dividing the contributions to $S(t)$ based on the solute position at the time of excitation does not recover a trend with cavity size. However, the same differences in ground and excited state solute

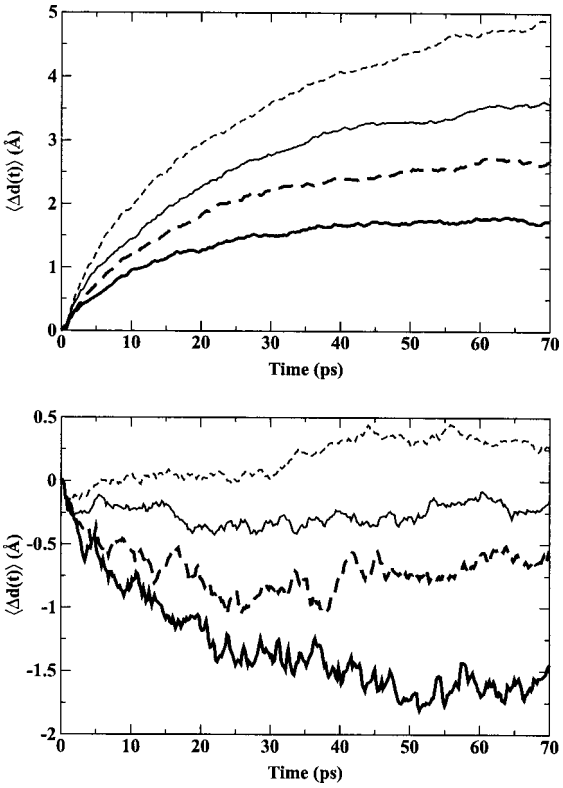

FIG. 8. The time-dependent change in solute position (shown in terms of the distance from the cavity wall) is plotted for (top panel) solutes in the first solvent shell next to the cavity wall when excited, and (bottom panel) the remaining solutes that are in the cavity interior when excited. The results are for a solute in CH_3I (ρ=1.4 g/cm^3) and are shown for R_{cav}=10 Å (thick solid line), 12 Å (thick dashed line), 15 Å (thin solid line), and 20 Å (thin dashed line).

position distributions that can be used to explain the dependence of the amplitudes, A_i, in the lower density results are also relevant here. Specifically, these amplitudes are primarily responsible for the lack of a trend. Note that the amplitudes corresponding to inertial dynamics, A_1, and solute motion, A_3 both increase with R_{cav} while A_2, which is presumed to be dominated by solvent reorientational dynamics, decreases (see Table I). At the same time, the decay times for inertial and reorientational solvation dynamics, τ_1 and τ_2, are essentially independent of cavity size (and the same as for the bulk solvent) while τ_3 is the same for R_{cav} =10 and 12 Å, but smaller for the 15 Å cavity. The relationship of the amplitude A_3 to the solute motion can be understood by examining the overlap between the solute ground and excited state distributions; this overlap decreases as the cavity size increases leading to greater solute motion. At the same time, the solute motion is more rapid for the largest cavity; this is in contrast to the lower density case but consistent with a less constrained solvent with increasing cavity size. The dependence of the amplitude A_2, associated primarily with solvent reorientational dynamics, on cavity size may be somewhat counterintuitive. However, this dependence is likely due to two factors: (1) The local solvent density felt by the solute is larger in the smaller cavities where the solvent layering is more extreme, see Fig. 6. This gives a solvation effect that increases as R_{cav} decreases. (2) The ground state solute position distribution becomes less localized near the cavity wall as the cavity size increases. This means more molecules are in the cavity interior upon excitation and the effective solvent density around the solute decreases as R_{cav} increases. Coupled with the decrease in A_2 with increasing cavity size is an increase in the amplitude for inertial dynamics, A_1. We also attribute this to the increased local solvent densities for smaller cavities combined with changes in the ground state solute position distribution which reduce the magnitude of the inertial response while enhancing the effect of solvent reorientational motion.

The fast time scale for solute motion, τ_{d1}, can be understood by examining the time-dependent solute position distributions after excitation (not shown). These distributions show solute motion only within the first solvent layer in the first 1.5 ps after excitation; virtually no solute movement between solvent layers is observed in the same time frame. Thus, the short-time solute motion, τ_{d1}, can be attributed to intralayer motion and the long-time component, τ_{d2}, to interlayer motion. This is in contrast to the ρ=1.4 g/cm^3 case where there is not a clearly observable separation of time scales between intralayer and interlayer solute motion.

The fast $\langle \Delta d(t) \rangle$ time scale and the middle $S(t)$ time scale coincide reasonably well. This ~2 ps decay is also similar to the long-time component in the bulk TDF simulation (see Table I). This implies that the solvent reorientation time is not strongly modified by confinement in this case but is accompanied by (or involves) some solute motion. There is not strong evidence for this model solute in CH_3I at these densities to support a two-state model[1] to describe the solvation dynamics. That is, no separation of time scales is observed for solutes near the cavity wall versus in the interior, only for solvent reorientational motion versus solute motion. However, the statistics for nonequilibrium trajectories beginning in the cavity interior are not sufficient to draw a definitive conclusion; it *is* clear that the multiple time scales observed in the total $S(t)$ cannot be attributed to different solvent reorientation times in the interior and near the cavity wall. Understanding how this result is related to properties of the cavity, solute dye molecule, and the solvent will require further study.

C. Comparisons with previous work

1. Theoretical work

There have been only a few theoretical studies of solvation dynamics in nanoconfined solvents,[30,34,35] most notably recent work by Nandi and Bagchi,[30] Senapati and Chandra,[35] and Faeder and Ladanyi.[34]

Senapati and Chandra[35] were apparently the first to simulate the solvation dynamics in a nanoconfined solvent. Their system consisted of a Stockmayer fluid in a spherical nanocavity (similar to the one used here) and a Lennard-Jones solute that is charged (excited state) or neutral (ground state). They found that the solvation dynamics in a nanocavity exhibits a similar inertial relaxation, though with a smaller amplitude, to that in the bulk solvent. In contrast, the long-time relaxation is ~4 times slower in the nanocavity than in the bulk. In their simulations the solute position was

held fixed and thus they did not observe solute motion that almost certainly would occur after excitation (which in this case corresponds to adding a charge).

More recently, Faeder and Ladanyi[34] simulated time-dependent fluorescence dynamics in model aqueous reverse micelles and hydrophobic cavities. Their hydrophobic cavity model,[33] developed by Linse and Halle,[32] is the same as that used here; the reverse micelle model consists of the same cavity framework with fixed anionic headgroups and mobile cationic counterions added.[33] The solvation dynamics were studied using an anionic diatomic probe molecule with symmetrically (ground state, $\mu=0$) or asymmetrically (excited state, $\mu=7.76$ D) distributed charge. They simulated the solvation dynamics for the first 2 ps after excitation and obtained results that were relatively independent of the size of the reverse micelle. In addition, the dynamics in the model reverse micelles were very similar to those in the hydrophobic cavities. Their solute molecule is negatively charged in both the ground and excited states likely giving position distributions that are quite similar. In addition, the present results indicate any solute motion would likely take place on a time scale longer than 2 ps.

Nandi and Bagchi[30] have used a multishell continuum model and molecular hydrodynamic theory to describe solvation dynamics in cyclodextrin cavities corresponding to experimental measurements.[20] In this case only a single solvation shell of water is contained with the solute inside the cavity and the size-dependence is not considered.

2. Experimental work

There has been a significant experimental work in recent years investigating solvation dynamics in nanoconfined systems.[3–27] One of the interesting and complicating aspects of these studies is the wide range of different systems that have been investigated. This can make the identification of general principles for confined solvent dynamics difficult; in this section we discuss previous work in the context of the present results with an emphasis on studies of cavity size-dependence. The reader is also referred to a recent review by Bhattacharyya and Bagchi.[29]

Levinger and co-workers have carried out extensive studies of solvation in reverse micelles by measuring steady-state spectra (electronic and vibrational) and time-dependent fluorescence.[9–15] Specifically, they have measured the time-dependent emission of Coumarin 343 in ionic aqueous, ionic formamide, and nonionic reverse micelles. They have investigated the effect of the solvent pool size, the surfactant, and the associated counterion. Typically they observe biexponential or triexponential decay in $S(t)$ with the shortest time scale ($<$300 fs) corresponding to inertial dynamics. The longest time scale ranges from a few picoseconds[9] to hundreds of picoseconds.[10] One consistent conclusion of their studies is that there is not a one-to-one correspondence between steady-state spectra and the time-dependent Stokes shift function, $S(t)$: "...steady-state spectroscopy may not always be a good predictor for dynamical behavior."[14]

Bhattacharyya and co-workers have measured the time-dependent fluorescence of the dye molecule, Coumarin 480, in solventless zeolites,[4] aqueous micelles[5] and reverse micelles,[6] in water pools in a sol-gel matrix,[7] and vesicles.[8] They found that the long-time solvation dynamics depend strongly on the environment with a long-time decay of ~0.8 ns in the sol-gel matrix,[7] 0.6–2.4 ns in micelles (using different surfactants),[5] 8–12 ns in reverse micelles,[6] 11 ns in vesicles,[8] and ~15.4 ns in the solventless zeolites.[4] (The solvent relaxation dynamics for Coumarin 480 in bulk aqueous solution takes place in 310 fs.[20]) In the case of reverse micelles they investigated two water pool sizes and found $S(t)$ exhibits a single 8 ns decay for the smaller water pool and a biexponential decay of 1.7 and 12 ns for the larger pool.[6] (Their time resolution is ~80 ps.)

Sarkar and co-workers have investigated the solvation dynamics of Coumarin 490 in aqueous reverse micelles and Coumarin 152A in acetonitrile and methanol reverse micelles.[22] In all cases they find biexponential decay of $S(t)$ with the fast decay ~0.5–1.7 ns and the long-time decay 7.6–15.5 ns. In the aqueous reverse micelles the longest decay time was essentially independent of the water pool size and the shorter time constant was smaller for the larger solvent pool. Interestingly, they found for Coumarin 152A in acetonitrile reverse micelles solvation times that were essentially independent of solvent pool size; this is not observed in aqueous or methanol reverse micelles. This is consistent with our results for CH_3I, another nonhydrogen bonding solvent.

Baumann *et al.* have investigated solvation dynamics in sol-gels with pore diameters of 25–75 Å.[16,17] They measured the steady-state spectra and time-dependent Stokes shift of nile blue and Coumarin 153 (C153) in ethanol inside the sol-gel pores. In the case of nile blue (a cationic dye with a negative counterion) they found a small blueshift in the steady-state absorption spectrum and a redshift in the fluorescence spectrum with increasing pore diameter (50 vs 75 Å).[16] For C153 (a neutral molecule) the absorption spectrum was unchanged and the fluorescence redshifted between 25 and 50 Å pores.[17] The results for the neutral C153 molecule are consistent with our simulations; spectral shifts for charged solutes such as nile blue can display distinctly different properties.[52] For both molecules they found $S(t)$ exhibited a triexponential decay (they could not resolve any subpicosecond component to the dynamics) in both bulk and confined solutions; the fastest components were on the time scale of a few picoseconds while the slower ones were tens of picoseconds, the longest being ~100 ps. The solvation dynamics slowed significantly upon confinement (and were slowest for the smallest pores). Interestingly they found for C153 the fastest decay time (~1.7 ps) was roughly the same for the bulk and 25 and 50 Å pores whereas the two longer decay times were reduced as the pore size was increased. In contrast, all decay times were reduced with increasing pore size for nile blue. In addition, the amplitudes of the different decay components changed with pore size; this was not true for nile blue. Further, they infer for C153 (from differences between the static and dynamic Stokes shifts) a decreasing inertial component with decreasing pore size. Thus, the results for C153 are generally consistent with our simulations while those for nile blue exhibit distinct differences. Baumann *et al.* proposed an enhanced polarization field model

and a steric hindrance model to account for the observed results.[16]

Clearly our model system does not represent the electrostatic interactions and flexibility present in the ''cavity'' wall of a reverse micelle or even a sol-gel matrix and we have not used water (or ethanol) as the solvent. However, it is interesting to examine the general features in our results that are also observed in experimental measurements. These include (1) the Stokes shift typically increases with increasing solvent pool size, (2) $S(t)$ decays on multiple time scales, and (3) the amplitudes, A_i in Eq. (4.1), display a nonmonotonic dependence on solvent pool size in some cases. Key differences include (1) in most, though not all, cases experiments observe consistent redshifts in the absorption spectra, and (2) they see a biexponential decay of $S(t)$ in some cases. Differentiating the generic solvation properties of confined solvents from those dependent on cavity characteristics will require additional theoretical and experimental work.

VI. CONCLUDING REMARKS

The time-dependent fluorescence of a model diatomic molecule with a charge transfer electronic transition in CH_3I confined in spherical cavities has been simulated by nonequilibrium molecular dynamics. The effects of cavity size and solution density have been explored.

Time decay of the normalized Stokes shift function, $S(t)$, is triexponential. The three time scales can be roughly attributed to inertial motion ($<$300 fs), solvent reorientational dynamics ($\sim$1.5–3 ps), and solute motion toward the cavity interior ($\sim$15–40 ps). These simulations confirm a prediction made previously that diffusive solute motion can be observed in the time-dependent fluorescence of solutes in nanoconfined solvents.[45] The solute motion that is observable in the long-time component of $S(t)$ is slower the larger the solution density. The time-dependent average solute position is single-exponential at the low density considered here but biexponential at the higher density.

While the Stokes shift increases with the cavity radius, the normalized Stokes shift function $S(t)$, Eq. (3.1), does not show a consistent trend with cavity size. Ultimately this is a result of the changes in the solute molecule position distribution with cavity size in the ground and excited states as well as the local solvent densities. These affect the amplitudes of the different time-components of $S(t)$. In the low density case, ρ=1.4 g/cm^3, a trend with cavity size can be recovered by dividing the nonequilibrium trajectories into those starting near and away from the cavity wall. The present results indicate that time-dependent fluorescence measurements may not necessarily be indicative of cavity size, even when the steady-state fluorescence spectra are.

It remains for future studies to determine exactly how generic the role of solute motion is in time-dependent fluorescence measurements. It is likely that cavity properties (e.g., shape, roughness, surface functionality), solute molecule characteristics (e.g., size, dipole moment changes), and solvent (e.g., size, polarity, hydrogen bonding ability) will all have an effect. However, the present simulations indicate that the combination of position-dependent solvation properties of nanoconfined solvents and significant changes in charge distributions of solutes means that solute motion should be considered in interpreting TDF experiments. More generally, these results have implications for charge transfer reactions (e.g., electron or proton transfer) in confined solvents where solute motion may be a component of the reaction coordinate; this is an area we are currently investigating.

ACKNOWLEDGMENTS

I thank Professor Carey K. Johnson, Professor Brian B. Laird, and Professor Xueyu Song for useful discussions. This work was supported by the Chemical Sciences, Geosciences and Biosciences Division, Office of Basic Energy Sciences, Office of Science, U.S. Department of Energy.

[1] J. Zhang and J. Jonas, J. Phys. Chem. **97**, 8812 (1993); J.-P. Korb, S. Xu, and J. Jonas, J. Chem. Phys. **98**, 2411 (1993); J.-P. Korb, L. Malier, F. Cros, S. Xu, and J. Jonas, Phys. Rev. Lett. **77**, 2312–2315 (1996); J.-P. Korb, S. Xu, F. Cros, L. Malier, and J. Jonas, J. Chem. Phys. **107**, 4044 (1997).
[2] B. J. Loughnane and J. T. Fourkas, J. Phys. Chem. B **102**, 10288 (1998); B. J. Loughnane, A. Scodinu, and J. T. Fourkas, *ibid.* **103**, 6061 (1999); B. J. Loughnane, R. A. Farrer, A. Scodinu, T. Reilly, and J. T. Fourkas, *ibid.* **104**, 5421 (2000); R. A. Farrer and J. T. Fourkas, Acc. Chem. Res. **36**, 605 (2003).
[3] C. Streck, Y. B. Mel'nichenko, and R. Richert, Phys. Rev. B **53**, 5341 (1996); R. Richert, *ibid.* **54**, 15762 (1996).
[4] K. Das, N. Sarkar, S. Das, A. Datta, and K. Bhattacharyya, Chem. Phys. Lett. **249**, 323 (1996).
[5] N. Sarkar, A. Datta, S. Das, and K. Bhattacharyya, J. Phys. Chem. **100**, 15483 (1996); A. Datta, D. Mandal, S. K. Pal, and K. Bhattacharyya, J. Phys. Chem. B **101**, 10221 (1997).
[6] N. Sarkar, K. Das, A. Datta, S. Das, and K. Bhattacharyya, J. Phys. Chem. **100**, 10523 (1996).
[7] S. K. Pal, D. Sukul, D. Mandal, S. Sen, and K. Bhattacharyya, J. Phys. Chem. B **104**, 2613 (2000).
[8] A. Datta, S. K. Pal, D. Mandal, and K. Bhattacharyya, J. Phys. Chem. B **102**, 6114 (1998).
[9] R. E. Riter, D. M. Willard, and N. E. Levinger, J. Phys. Chem. B **102**, 2705 (1998).
[10] D. Pant, R. E. Riter, and N. E. Levinger, J. Chem. Phys. **109**, 9995 (1998).
[11] R. E. Riter, E. P. Undiks, J. R. Kimmel, and N. E. Levinger, J. Phys. Chem. B **102**, 7931 (1998).
[12] D. M. Willard, R. E. Ritter, and N. E. Levinger, J. Am. Chem. Soc. **120**, 4151 (1998); D. M. Willard and N. E. Levinger, J. Phys. Chem. B **104**, 11075 (2000).
[13] D. Pant and N. E. Levinger, Langmuir **16**, 10123 (2000).
[14] R. E. Riter, E. P. Undiks, and N. E. Levinger, J. Am. Chem. Soc. **120**, 6062 (1998).
[15] R. E. Riter, J. R. Kimmel, E. P. Undiks, and N. E. Levinger, J. Phys. Chem. B **101**, 8292 (1997).
[16] R. Baumann, C. Ferrante, F. W. Deeg, and C. Bräuchle, J. Chem. Phys. **114**, 5781 (2001).
[17] R. Baumann, C. Ferrante, E. Kneuper, F. W. Deeg, and C. Bräuchle, J. Phys. Chem. A **107**, 2422 (2003).
[18] J. Zhang and F. V. Bright, J. Phys. Chem. **95**, 7900 (1991).
[19] C. H. Cho, M. Chung, J. Lee, T. Nguyen, S. Singh, M. Vedamuthu, S. Yao, J.-B. Zhu, and G. W. Robinson, J. Phys. Chem. **99**, 7806 (1995).
[20] S. Vajda, R. Jimenez, S. J. Rosenthal, V. Fidler, G. R. Fleming, and E. W. Castner, Jr., J. Chem. Soc., Faraday Trans. **91**, 867 (1995).
[21] K. Hara, H. Kuwabara, and O. Kajimoto, J. Phys. Chem. A **105**, 7174 (2001).
[22] P. Hazra and N. Sarkar, Chem. Phys. Lett. **342**, 303 (2001); P. Hazra, D. Chakrabarty, and N. Sarkar, Chem. Phys. Lett. **358**, 523 (2002).
[23] B. L. Bales, R. Ranganathan, and P. C. Griffiths, J. Phys. Chem. B **105**, 7465 (2001).
[24] R. M. Dickson, D. J. Norris, Y.-L. Tzeng, and W. E. Moerner, Science **274**, 966 (1996).
[25] H. Wang, A. M. Bardo, M. M. Collinson, and D. A. Higgins, J. Phys.

Chem. B **102**, 7231 (1998); E. Mei, A. M. Bardo, M. M. Collinson, and D. A. Higgins, *ibid.* **104**, 9973 (2000).
[26] S. Das, A. Datta, and K. Bhattacharyya, J. Phys. Chem. A **101**, 3299 (1997); D. Mandal, S. K. Pal, and K. Bhattacharyya, *ibid.* **102**, 9710 (1998); S. K. Pal, D. Mandal, and K. Bhattacharyya, J. Phys. Chem. B **102**, 11017 (1998).
[27] B. Valeur and E. Bardez, in *Structure and Reactivity in Reverse Micelles*, edited by M. P. Pileni (Elsevier, New York, 1989), pp. 103–122.
[28] *Molecular Dynamics in Restricted Geometries*, edited by J. Klafter and J. M. Drake (Wiley, New York, 1989); M. Schoen, *Computer Simulation of Condensed Phases in Complex Geometries* (Springer-Verlag, New York, 1993).
[29] K. Bhattacharyya and B. Bagchi, J. Phys. Chem. A **104**, 10603 (2000).
[30] N. Nandi and B. Bagchi, J. Phys. Chem. **100**, 13914 (1996).
[31] D. Brown and J. H. R. Clarke, J. Phys. Chem. **92**, 2881 (1988).
[32] P. Linse, J. Chem. Phys. **90**, 4992 (1989); P. Linse and B. Halle, Mol. Phys. **67**, 537 (1989).
[33] J. Faeder and B. M. Ladanyi, J. Phys. Chem. B **104**, 1033 (2000).
[34] J. Faeder and B. M. Ladanyi, J. Phys. Chem. B **105**, 11148 (2001).
[35] S. Senapati and A. Chandra, J. Chem. Phys. **111**, 1223 (1999).
[36] S. Senapati and A. Chandra, J. Phys. Chem. B **105**, 5106 (2001).
[37] C. H. Turner, J. K. Brennan, J. K. Johnson, and K. E. Gubbins, J. Chem. Phys. **116**, 2138 (2002).
[38] See, e.g., J. H. Fendler, J. Phys. Chem. **84**, 1485 (1980); *Structure and Reactivity in Reverse Micelles*, edited by M. P. Pileni (Elsevier, New York, 1989).
[39] C. J. Brinker and G. W. Scherer, *Sol-Gel Science: The Physics and Chemistry of Sol-Gel Processing* (Academic, New York, 1990).
[40] See, e.g., J. Rebek, Jr., Acc. Chem. Res. **32**, 278 (1999); L. R. MacGillivray and J. L. Atwood, Adv. Supramolec. Chem. **6**, 157 (2000); J. W. Steed and J. L. Atwood, *Supramolecular Chemistry* (Wiley, New York, 2000).
[41] A recent example is L.-Q. Gu, S. Cheley, and H. Bayley, Science **291**, 636 (2001).
[42] See, e.g., D. E. De Vos, M. Dams, B. F. Sels, and P. A. Jacobs, Chem. Rev. **102**, 3615 (2002).
[43] R. A. Marcus, Annu. Rev. Phys. Chem. **15**, 155 (1964); M. D. Newton and N. Sutin, *ibid.* **35**, 437 (1984).
[44] See, e.g., R. A. Marcus, Proc. Electrochem. Soc. **80**, 1 (1980); A. Warshel, *Computer Modelling of Chemical Reactions in Proteins and Solution* (Wiley, New York, 1991); J. Juanós i Timoneda, and J. T. Hynes, J. Phys. Chem. **95**, 10431 (1991); P. L. Geissler, C. Dellago, D. Chandler, J. Hutter, and M. Parrinello, Science **291**, 2121 (2001).
[45] W. H. Thompson, J. Chem. Phys. **117**, 6618 (2002).
[46] R. M. Stratt and M. Maroncelli, J. Phys. Chem. **100**, 12981 (1996).
[47] These simple energetic arguments, while ultimately decisive, are modulated by a geometric one: The space available for a solute molecule a distance r from the cavity center is proportional to r^2.
[48] A. Warshel, *Computer Modelling of Chemical Reactions in Proteins and Solution* (Wiley, New York, 1991).
[49] F. F. M. Freitas, F. M. S. S. Fernandes, and B. J. C. Cabral, J. Phys. Chem. **99**, 5180 (1995).
[50] *Handbook of Chemistry and Physics*, edited by R. C. Weast, 52nd ed. (The Chemical Rubber Company, Cleveland, OH, 1971).
[51] S. D. Bond, B. J. Leimkuhler, and B. B. Laird, J. Comput. Phys. **151**, 114 (1999).
[52] See, e.g., D. Laage, W. H. Thompson, M. Blanchard-Desce, and J. T. Hynes, J. Phys. Chem. A **107**, 6032 (2003).